HiSST: 2nd International Conference on
High-Speed Vehicle Science & Technology
20-24 April 2020, Bruges, Belgium

Shockwave boundary layer interaction of laminar/transitional flow past a sharp fin

Tobias Ecker[†], *Jan Martinez Schramm* [‡], *Leni Schmidt*[§], *Divek Surujhlal*[¶], *Alexander Wagner*[‖]

Abstract

Ever since NASA's X-plane program had developed demonstrators (X-15) pushing into the hypersonic high altitude flight regimes, the effects of shock impingement and interference on local aerodynamic heating have been a key issue for the design of hypersonic flight concepts. Currently DLR is involved in several flight experiments, one of which is STORT which focuses on aerothermal loads on hot structures. One essential structure flown on the STORT flight experiment is the fins experiment on the third stage. The fins were investigated both on the vehicle, in windtunnels in Cologne and Göttingen but also numerically. For the windtunnel experiment in the HEG (High Enthalpy Shock Tunnel Göttingen) the object of investigation is a plate mounted fin which scales 1:2 to the flight hardware. The fin-induced shock boundary layer interaction (SWBLI) on the plate leads to increased thermal loads. The heat flux on the flat plate and fin are investigated using temperature sensitive paints (TSP). For the current study the flow on the plate and around the fin is studied for two HEG freestream conditions at Mach 7.4 using RANS CFD. CFD calculations at both 0 deg AoF and 15 deg AoF were performed and compared for flow topology and turbulence model influence. For 2 configurations first preliminary comparisons between experimental and CFD data were conducted. While the XIII freestream condition compares well between experiment and CFD, the XV freestream condition which shows clear signs of transitional flow exhibits rather complex physical phenomena which require further investigation, both experimentally and numerically.

Keywords: *SWBLI, shock, fin, heat flux, CFD*

Nomenclature

Latin
AoF – angle of fin
M – Mach number
Re – Reynolds number
T – Temperature
Q – Heat flux

Greek
ρ – Density

Subscripts
w – Wall
0 – total conditions

1. Introduction

Ever since NASA's X-plane program had developed demonstrators (X-15) pushing into the hypersonic high altitude flight regimes, the effects of shock impingement and interference on local aerodynamic heating have been a key issue for the design of hypersonic flight concepts[1] and are still a programmatic inspiration for current and future work[2]. Currently DLR is involved in several flight experiments, among them CALLISTO which is a first stage demonstrator, REFEX which has a main focus on guidance and navigation and STORT[3] which focuses on aerothermal loads on hot structures. STORT (Schlüsseltechnologien für hochenergetische Rückkehrflüge von Trägerstufen / Key Technologies for High Speed Return Flights

[†] *German Aerospace Center, Institute of Aerodynamics and Flow Technology, tobias.ecker@dlr.de*
[‡] *German Aerospace Center, Institute of Aerodynamics and Flow Technology, jan.martinez@dlr.de*
[§] *German Aerospace Center, Institute of Aerodynamics and Flow Technology, leni.schmidt@dlr.de*
[¶] *German Aerospace Center, Institute of Aerodynamics and Flow Technology, divek.surujhlal@dlr.de*
[‖] *German Aerospace Center, Institute of Aerodynamics and Flow Technology, alexander.wagner@dlr.de*

of Launcher Stages) uses a three-stage sounding rocket configuration and will be flying on a suppressed trajectory in order to increase integral heat load on structures [3, 4] . One essential structure flown on the STORT flight experiment is the fins experiment on the third stage. The fins were investigated both on the vehicle, in windtunnels in Cologne and Göttingen but also numerically. For the windtunnel experiment in the HEG (High Enthalpy Shock Tunnel Göttingen) the object of investigation is a plate mounted fin which scales 1:2 to the flight hardware. The fin induced shock boundary layer interaction (SWBLI) on the plate leads to increased thermal loads. The heat flux on the flat plate and fin are investigated using temperature sensitive paints (TSP[5–7]). Within the range of canonical SWBLI configurations[8] the STORT fin configuration is a special case of the fin type as it combines a sharp fin with a planar section more representative of flight hardware albeit without the sweep commonly found in hypersonics. Similar planar fins have been studied numerically and experimentally for fins mounted both on flat as well as cylindrical surfaces for the mean flow topology of SWBLI by Pickles et al.[9]. The study by Pickles et al. is an important link between the canonical cases and application to flight and while the cylindrical surface has an impact on separation and inviscid shock curvature, the overall flow structure has large similarities between the planar and cylindrical cases. Previous proof-of-principle measurements using TSP were conducted in the AEDC wind tunnel by Smith et al[10] for a 30 deg wedge on an 33.5 deg angled plate (wedge). Based on the temperature results the authors demonstrated successful boundary layer tripping and the influence of SWBLI on surface temperatures.

For the current study the flow on the plate and around the fin is studied for two HEG conditions at Mach 7.4 using RANS CFD for multiple turbulence models and compared to experimental heat flux results obtained in the HEG via a TSP method.

2. Windtunnel and experiment

2.1. HEG

Experiments were conducted in the free-piston-driven High Enthalpy Shock Tunnel Göttingen (HEG). HEG was commissioned and further developed in order to duplicate flight conditions for the investigation of the flow around entry and reentry vehicles. The freestream conditions pertinent to this work are representative of around 30 km altitude at Mach 7.4. The wall-to-stagnation temperature ratios were $T_w/T_0 \approx 0.1$ with stagnation enthalpies of $h_0 \approx 3.1\ MJ/kg$. Higher stagnation enthalpy test conditions are additionally available to investigate the influence of high-temperature effects such as chemical and thermal relaxation on the aerothermodynamics of entry or reentry vehicles. Further detailed information on HEG is provided in the given reference by DLR [11]. The TSP diagnostic was used to obtain the surface heat flux distribution on the flat plate model and on the fin. The base layer was applied to the fin and a section of the flat plate on which the TSP layer was applied. Layer thickness of the TSP was estimated at approximately 3 μm. More details of TSP composition development can be found in the works of Schramm et al. and Ozawa et al. [5, 6]. For each pixel imaged from the measurement surfaces, a temporal integration of the temperature history was performed to obtain heat flux [12]. This method required an in-situ calibration of the base layer following the procedures as detailed by Schramm et al. [6] and Ozawa et al. [5]. The estimated uncertainty in the derived heat-flux was 5 % [5].

2.2. Flow conditions

The investigated flow conditions are listed in table 1. Both conditions are at M=7.4 but leverage flow conditions from laminar (XIII) to transitional/turbulent (XV) at approximately double the Reynolds number. For condition XV the boundary layer (BL) is tripped in the experiment using roughness elements. For all studies the wall temperature was assumed to be 300 K.

2.3. Fin geometry

The CAD geometry of the fin is derived from the flight geometry as communicated during the project phase. Due to the dimensions of the HEG test section the fin is scaled to 1:2 of the flight geometry. A CAD drawing of the fin geometry is shown in figure 1a. A overview of the fin plate geometry is shown in figure 1b. At zero angle of attack (called AoF: angle of fin from hereon) the fin leading edge (LE) is located 250 mm downstream from the leading edge of the flate plate mounted in the test section. The center of rotation of the fin is located at 50% fin length. The radius of the plate LE is 0.1 mm, the length of the carrier plate is 600 mm and the width is 340 mm.

Table 1. HEG tunnel conditions [11].

Cond.	XIII (H3.3R3.7)	XV (H3.0R6.4)
M	7.4	7.4
Re_m	$3.7\,10^6$ 1/m	$6.4\,10^6$ 1/m
ρ	25.9 g/m^3	43.2 g/m^3
T_0	2740 K	2582 K
flow	laminar	transitional

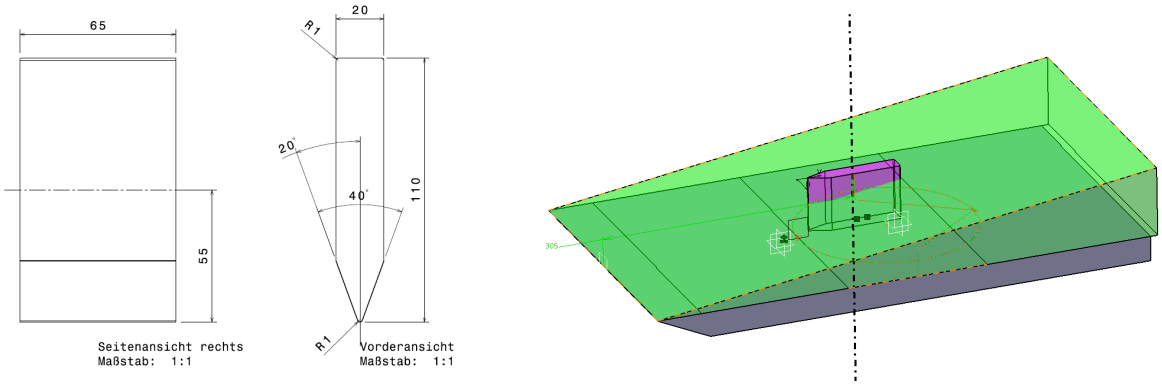

(a) Drawing of the fin geometry.

(b) CAD model, green transparent surfaces indicates shock from plate LE.

Figure 1. Experiment geometry.

2.3.1. Possible configurations

The fin on plate configuration allows to cover multiple (albeit not completely independent) flow deflection angles by turning the fin. The potential flow deflection angles are summarized in table 2. For the experimental entries only AoF of zero deg and 15 deg are available and therefore these are the cases the numerical study focuses on. For AoF of zero deg the deflection angles are symmetric at 20 deg whereas for the AoF 15 deg case both a effective 5 deg deflection and a 35 deg deflection are present.

Table 2. Deflection matrix

AoF	angle L	angle R
→**0 deg**	20 deg	20 deg
5 deg	15 deg	25 deg
10 deg	10 deg	30 deg
→**15 deg**	5 deg	35 deg

3. CFD study

3.1. CFD code and boundary conditions

All numerical investigations in the framework of the present study were performed with the hybrid structured/unstructured DLR Navier-Stokes solver TAU[13], which is validated for a wide range of steady and unsteady sub-, trans- and hypersonic flow cases. The TAU code is a second order finite-volume solver for the Euler and Navier-Stokes equations in the integral form using eddy-viscosity, Reynolds-stress or detached- and large eddy simulation for turbulence modeling. The AUSMDV flux vector splitting scheme was applied together with MUSCL gradient reconstruction to achieve second order spatial accuracy.

3.2. 3D study fin

3.2.1. Calculation matrix

The final calculation matrix is displayed in table 3. Asides from the laminar solver, both the Spalart-Allmaras (SA original)[14] and Menter k-ω SST[15] turbulence models were used. For selected cases also the Menter k-ω SST modell with a prescribed transition line was used.

Table 3. Calculation matrix

Cond.	AoF	laminar	SA*	k-ω SST	k-ω SST (forced transition)
XIII	0 deg	+	+	+	
XIII	15 deg	+	+		
XV	0 deg	+	+	+	
XV	15 deg	+	+	+	+ (5 mm from LE)

3.2.2. Mesh

For the 3D study the plate and fin configuration are generated as a CAD model in ”free flight” configuration. This means no mounts or other wind tunnel hardware are present within the geometry. The mesh configuration is visualized in figure 2. The leading edge of fin and plate were meshed with a structured surface grid in order to obtain ideal boundary layer conditions. Grid refinement volumes concentrate on the regions with shocks and expansions, as well as close to the regions of SBLI. Depending on AoF and case grid sizes between 8.5 and 12 Million points were generated. Comparisons on the influence of laminar flow /transition modeling / and different turbulence models for a 2D case were conducted and used to determine the best approach on the flat plate grid construction.

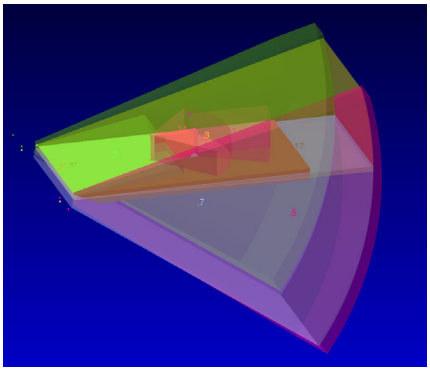

(a) CAD geometry and regions of refinement

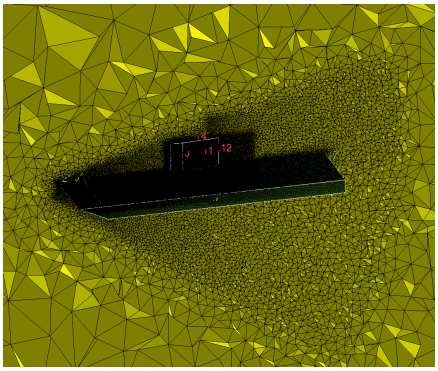

(b) overview mesh

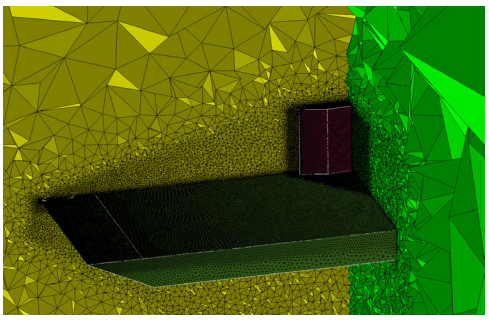

(c) mesh detail

Figure 2. Mesh generation.

3.2.3. Results XIII

The results for the laminar case at XIII condition are visualized in figures 3 and 4 for zero and 15 deg AoF respectively.

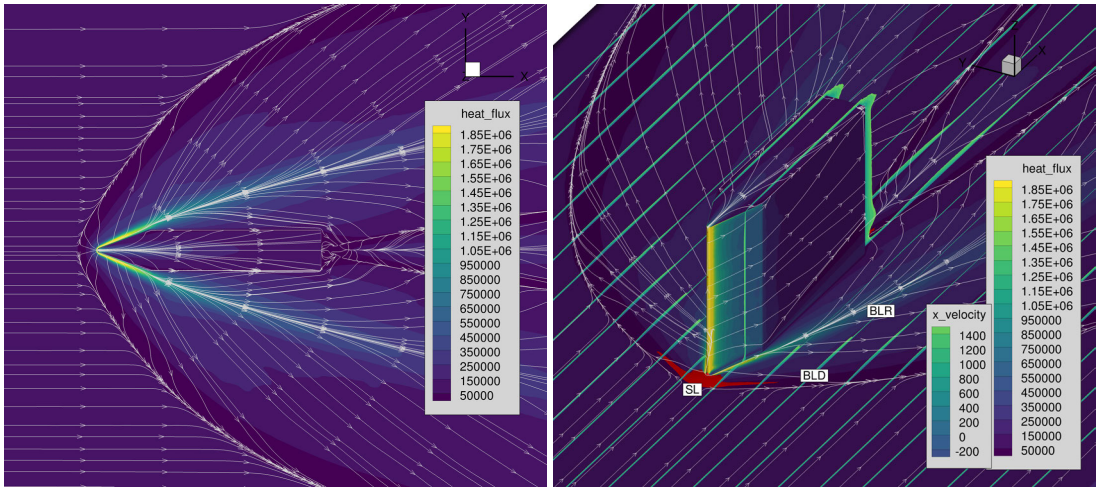

Figure 3. Cond. XIII Laminar: 0 deg AoF . Streamlines on the surface represent shear stress vectors, surface colors show heat flux, colored field planes show x-velocity. separation line (SL), boundary layer deformation (BLD), re-normalisation of boundary layer (BLR) / reattachement.

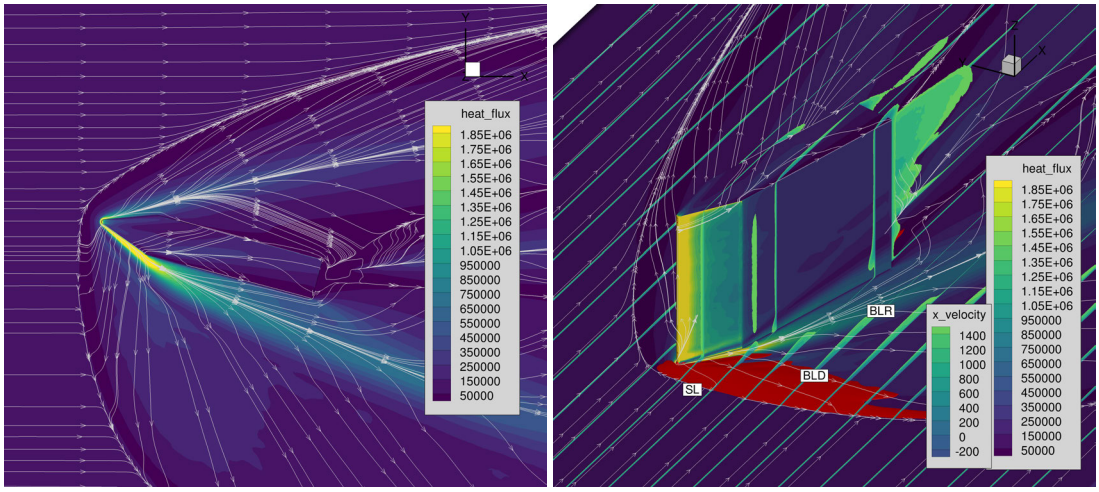

Figure 4. Cond. XIII Laminar: 15 deg AoF . Streamlines on the surface represent shear stress vectors, surface colors show heat flux, colored field planes show x-velocity. separation line (SL), boundary layer deformation (BLD), re-normalisation of boundary layer (BLR) / reattachement.

At zero AoF the boundary layer separation along the separation line (SL) in front of the fin is minimal. For the 15 deg AoF case the SBLI is dominated by a large area with a separated boundary layer (colored red) followed by region with a deformed boundary layer (BLD) which re-normalizes (BLR) near the expansion at the aft section of the fin. The general structure is similar to the structure presented by Knight et al.[16] for turbulent supersonic flow around a sharp fin, where SL represents the line of coalescence and BLR the line of divergence (attachment). As expected from previous work peak heat fluxes are located near the BLR.

A comparison of all laminar and turbulent cases for the XIII condition at 0 deg AoF in the top view of the plate is shown in figure 5. Clear differences are observable for the shape of the separation line between

the laminar and turbulent cases.

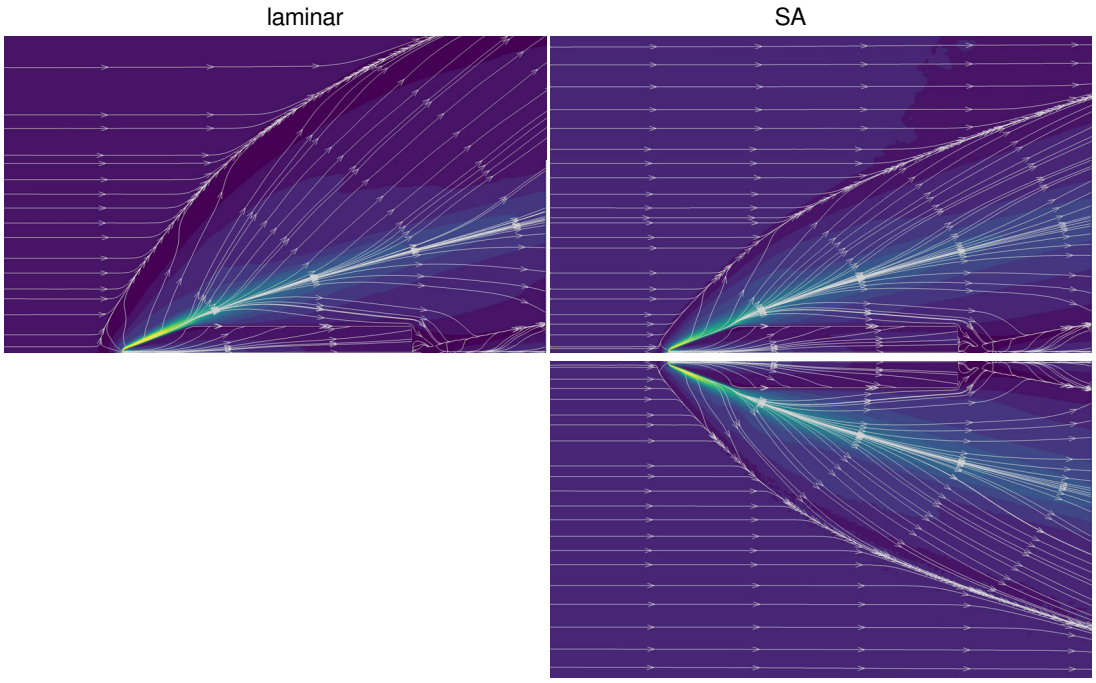

Figure 5. Cond. XIII Overview: 0 deg AoF. Streamlines on the surface represent shear stress vectors, surface colors show heat flux.

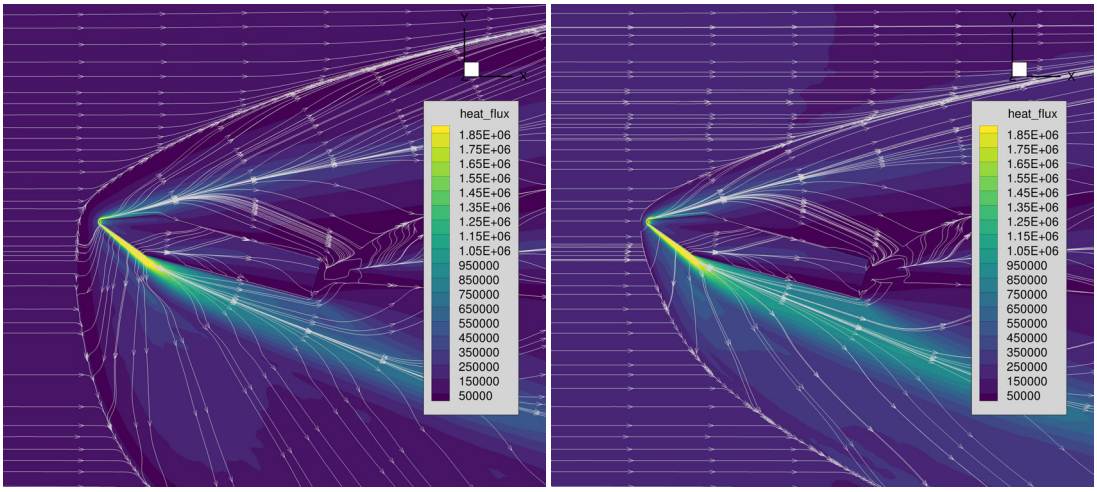

(a) laminar **(b)** SA

Figure 6. Cond. XIII Overview: 15 deg AoF. Streamlines on the surface represent shear stress vectors, surface colors show heat flux.

3.2.4. Results XV

The results for the transition/turbulent case at XV conditions are visualized in figures 7 and 8 for zero and 15 deg AoF respectively. Similar to the XIII condition there is, at zero AoF, boundary layer separation along

the separation line (SL) in front of the fin is minimal. For the 15 deg AoF case the SBLI is dominated by a large area with a separated boundary layer (colored red) followed by region with a deformed boundary layer (BLD) which re-normalizes (BLR) near the expansion at the aft section of the fin. Compared to the laminar XIII case the region of peak heat fluxes is increased and presents with high magnitudes.

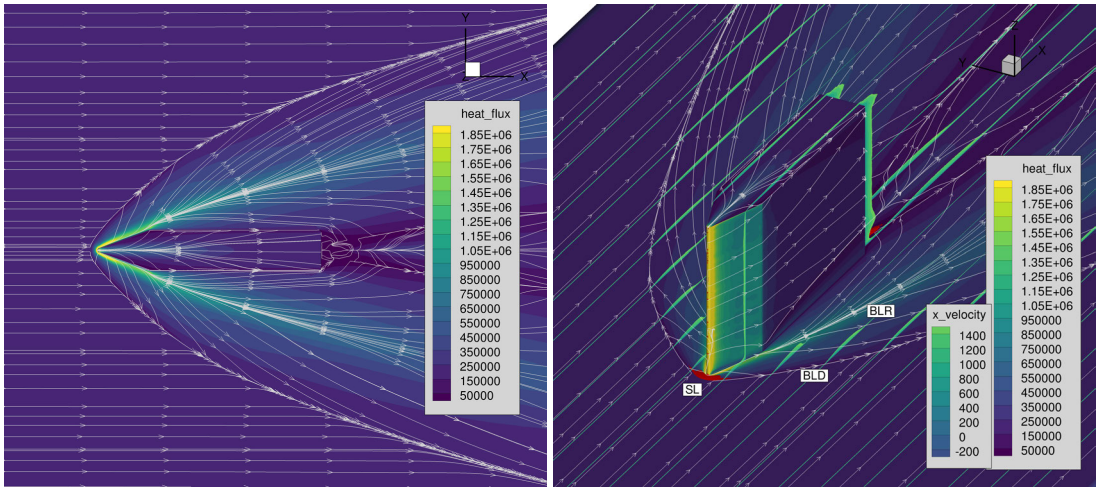

Figure 7. Cond. XV SA turbulence model: 0 deg AoF. separation line (SL), boundary layer deformation (BLD), re-normalisation of boundary layer (BLR) /reattachement .

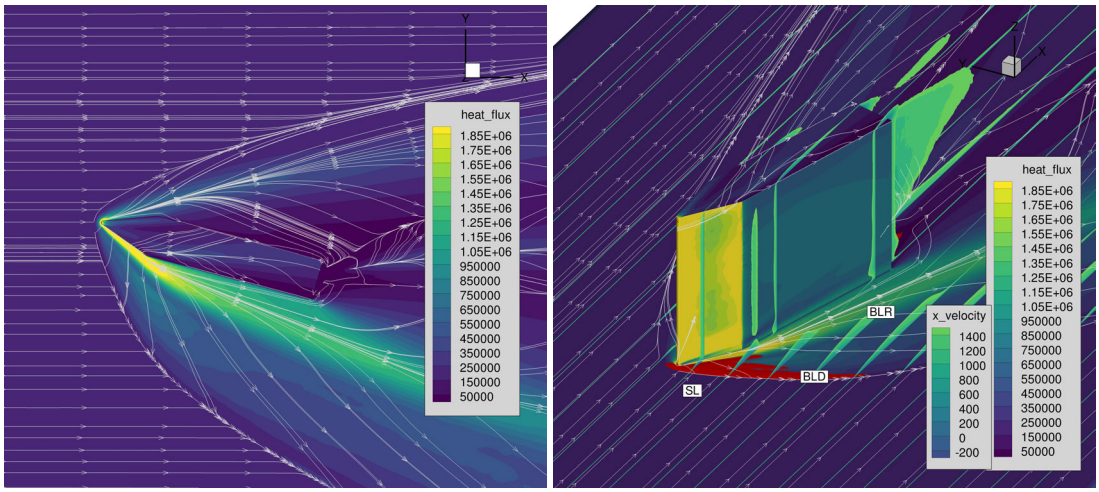

Figure 8. Cond. XV SA turbulence model: 15 deg AoF. separation line (SL), boundary layer deformation (BLD), re-normalisation of boundary layer (BLR) / reattachement .

A comparison of all laminar and turbulent cases for the XV condition in the top view of the plate is shown in figure 9. As before, clear differences are observable for the shape of the separation line between the laminar and turbulent cases. However, the differences in flow structure for the turbulent cases are indiscernible.

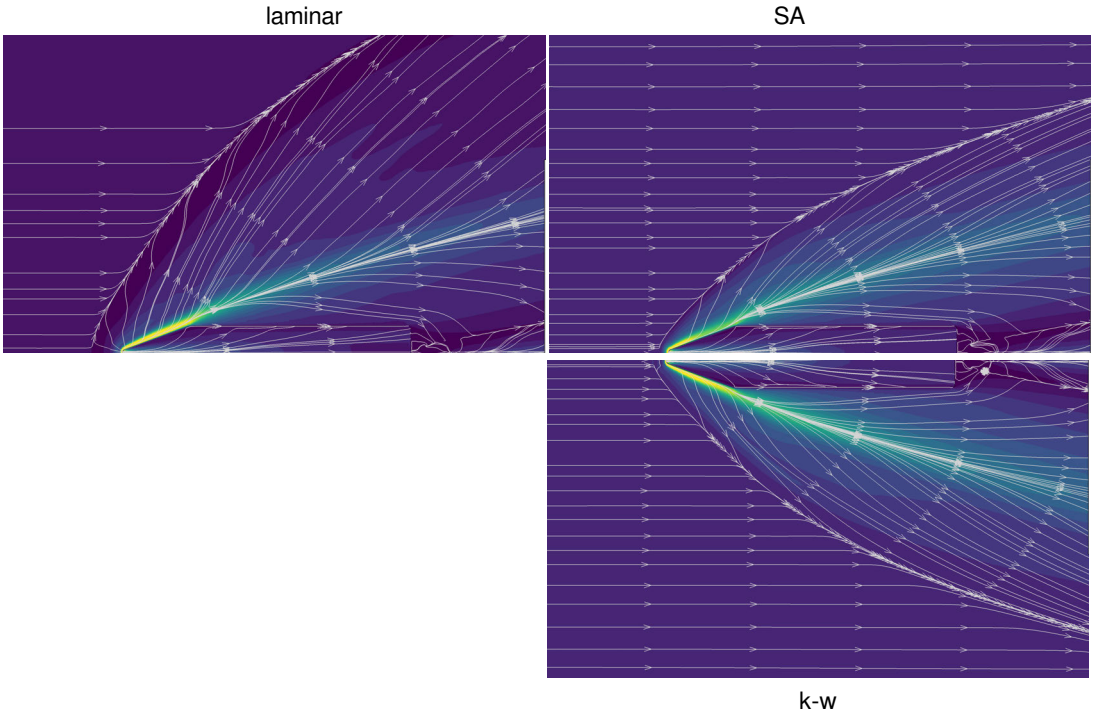

Figure 9. Cond. XV Overview: 0 deg AoF .

4. Comparison between experimental and numerical results

In difference to the CFD calculation, the experimental data is only available for part of the tested model due to viewing / camera limitations. Therefore comparisons are mainly made for the surfaces that are available in both datasets. The numerical domain and the experimental measurement domain are shown in figure 10 and figure 11 from a top down perspective. The different colors of the camera pixels represent different data sections from a 3D stitching process. The cone of influence drawn from the leading edge corner shows that effects from the limited span of the flat plate should be negligible.

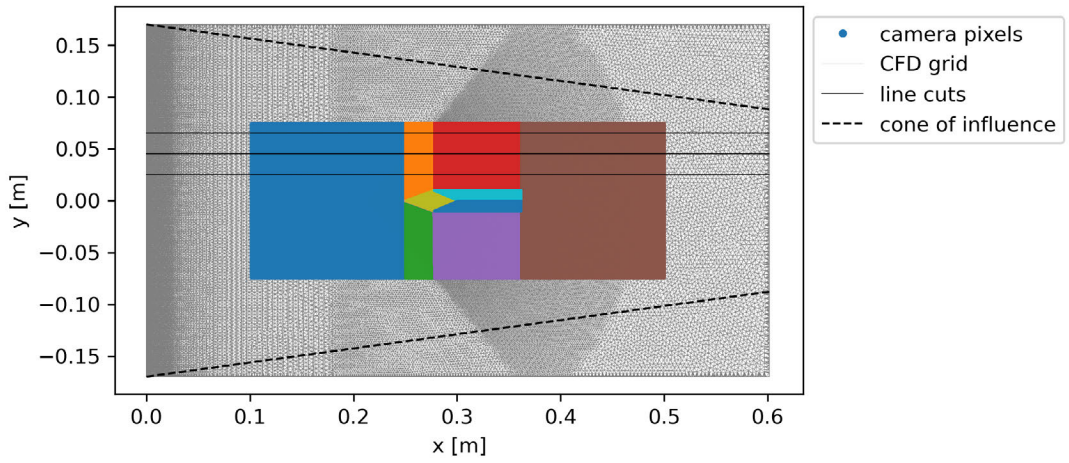

Figure 10. Top view on numerical and experimental domain - lines represent the location of data evaluation in the following analysis (y = 0.03, 0.05, 0.07 m) for the 0 deg AoF configuration.

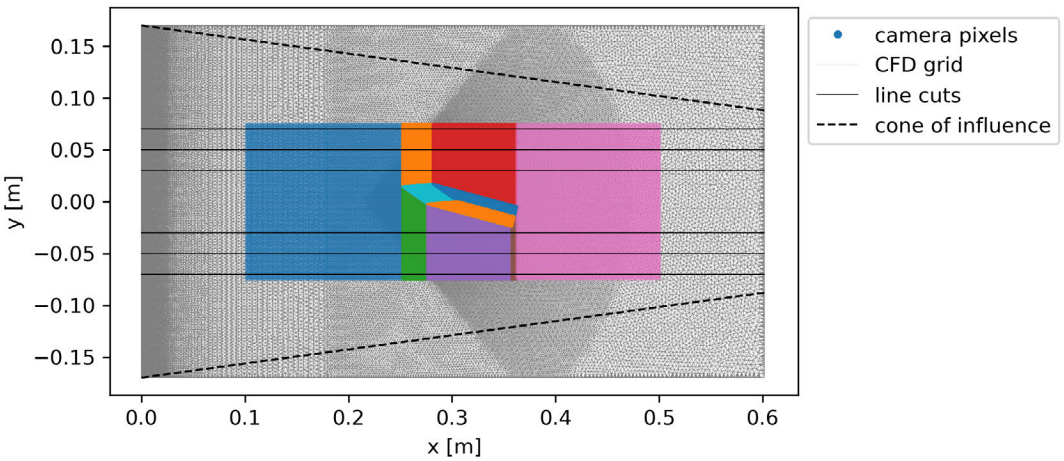

Figure 11. Top view on numerical and experimental domain - lines represent the location of data evaluation in the following analysis (y = $\mp$ 0.03, 0.05, 0.07 m) for the 15 deg AoF configuration.

4.1. SWBLI: XIII

The XIII HEG freestream condition is a laminar one. A comparison between experiment and the laminar CFD calculation is shown in figure 12 for both the isometric view and a top down view .

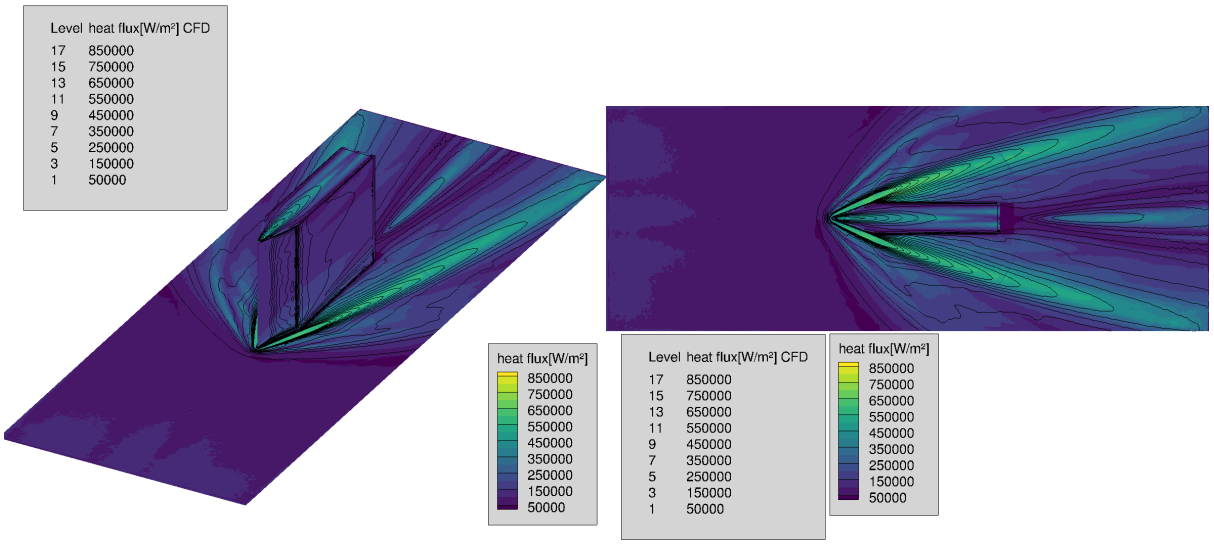

(a) XIII: laminar (iso) **(b)** XIII: laminar (top)

Figure 12. Comparison between CFD and experiment for entire measurement area for XIII condition.

It can be seen that there is a good comparison between experiment and numerical results on the flat plate section, but the high heat fluxes on the fin leading edge and the angled fin section predicted by theory and the CFD simulation are not present for the experiment. As these differences can not currently be explained the present analysis if focused on the flat plate (top) and the shock wave boundary layer interaction on the flat plate.

For a more quantitative comparison between experiment and the CFD results the heat flux at different y locations (shown in figure 10) is extracted. The results of this extraction is shown in figure 13a. For the purpose of this evaluation, but also to smooth out some of the noise and uncertainty in positioning, the data is averaged over 50–100 pixels. The numerical data is interpolated on to the data locations from the

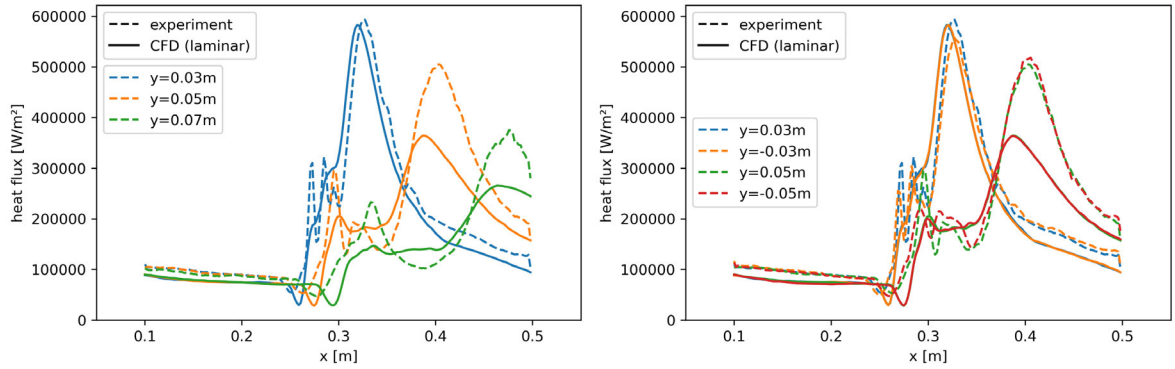

(a) data for y = 0.03, 0.05, 0.07. **(b)** data for y = ∓ 0.03, 0.05 on both sides of the fin.

Figure 13. Heat flux from experimental data and numerical data on constant y coordinates for condtion XIII and 0 deg AoF.

experiment and averaged in the exact same way. Especially for the location close to the centerline /close to the fin a y = 0.03 m, the experimental data and the numerical data are a close match both in magnitude and gradients. For the locations further away the CFD underpredicts the heatflux magnitude but follows the general trend seen in the experiment. A possible cause could be SWBLI induced transition which leads to higher heat flux downstream of the fin LE. The experimental data could be further analyzed (e.g surface heat flux fluctuations) to see if experimental evidence for for laminar/turbulent transition exists.

As the 0 deg AoF case is symmetric on the plate centerline, it is useful to look at profiles on both sides from the fin for both experiment and CFD data. This comparison is shown in figure 13b. While the CFD data is virtually symmetric, small (expected) differences are shown in the experimental data, however these deviations are very small and give additional confidence as to the general uncertainties within the experimental method.

4.2. SWBLI: XV

A similar comparison was made for the XV condition for the 15 deg AoF case. The comparison between experimental and numerical data for both laminar and turbulence models cases are shown in figure 14. Just like for the XIII condition, the fin heat flux distribution and the match between CFD data and experiment are still an open point and the analysis is limited to the top of the flat plate and the SBLI. Further one important aspect which is important to note is the occurrence of streaks in the heat flux distribution, mainly for the flat plate section before the fin, which is an indicator for the flow being in a transitional stage between laminar and turbulent flow.

Qualitatively speaking the turbulent CFD results are a closer match to the experimental data, showing similar shapes for the separation line and line of divergence for the side with the 35 deg deflection angle (negative y coordinate / bottom - marked with red arrow). For the 5 deflection angle (positive y coordinate / top - marked with red arrow) there is a slightly better match on top of the fin and in the area downstream of the blunt part of the fin the match between experiment and CFD is generally not as good.

For quantitative analysis line data for both positive coordinates (5 deg deflection) and negative coordinates (35 deg deflection) is extracted and plotted vs the experiment in figure 15 for SA turbulence model, k-ω SST and k-ω SST with transition turbulence model. From these comparisons the SA turbulence model reproduces the experimental data best for the 5 deg deflection (top) side. For the 35 deg deflection (bottom) side there is no good comparison between experiment and CFD peak heat fluxes. The heat flux values predicted by CFD are generally much higher then the data extracted from the experiment, but predict the location of the SWBLI correctly. The k-ω SST transition turbulence model is not shown as the onflow condition is not strictly at laminar levels and the transition model did not lead to improvement. On a further note, the experimental data for the XV condition has a much larger scatter in both the on flow as well as in

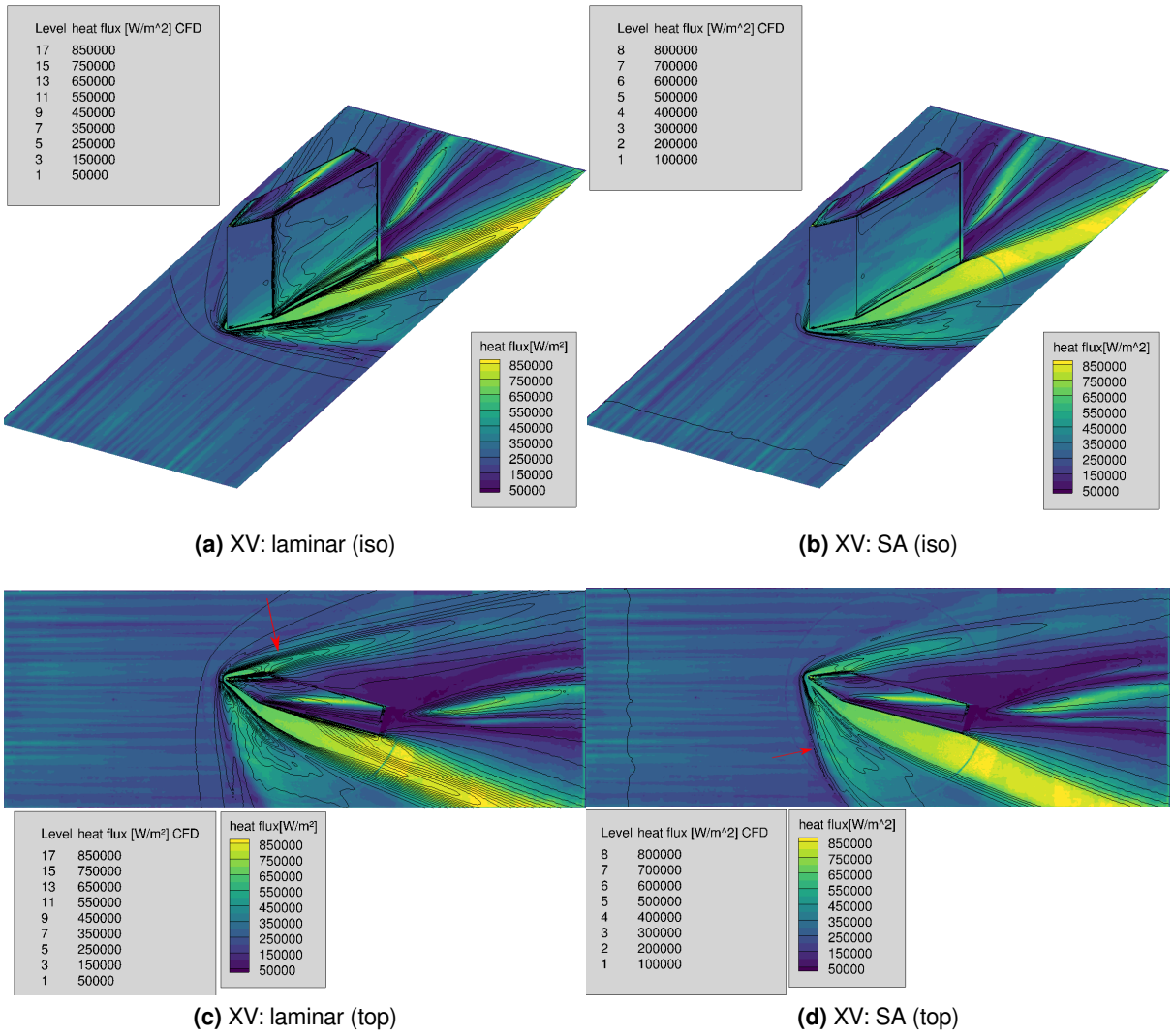

(a) XV: laminar (iso)

(b) XV: SA (iso)

(c) XV: laminar (top)

(d) XV: SA (top)

Figure 14. Comparison between CFD (laminar) and experiment for entire measurement area for XIII condition. Top section (in the top view) has an effective 5 deg deflection angle, bottom section (in the top view) has an effective 35 deg deflection angle.

the fin section. A possible explanation would be a saturation effect in the locations with peak heat fluxes. This explanation is supported by the lack of falloff between the y coordinates and the fact that for TSP high temperatures lead to a decrease in luminescence. Apart from the magnitudes the onset of the SWBLI enhanced heat fluxes including the dip near the separation line, as well as the fall off are predicted quite well - further indicating a sensitivity issue at the peaks.

5. Conclusions and Future Work

In this study the numerical work performed in support of the fin experiments in the HEG is described in detail. The object of investigation is a plate mounted fin which scales 1:2 to the fin flown in the STORT flight experiment. Using the DLR TAU solver the flow on the plate and around the fin is investigated for two HEG freestraem conditions using multiple turbulence models and fin angles. Comparisons on the influence of laminar flow /transition modeling / and different turbulence models for a 2D case were conducted and used to determine the best approach on the flat plate grid construction. For the 3D fin geometry, CFD calculations at both 0 deg AoF and 15 deg AoF (the same conditions and configuration as investigated in the HEG) were

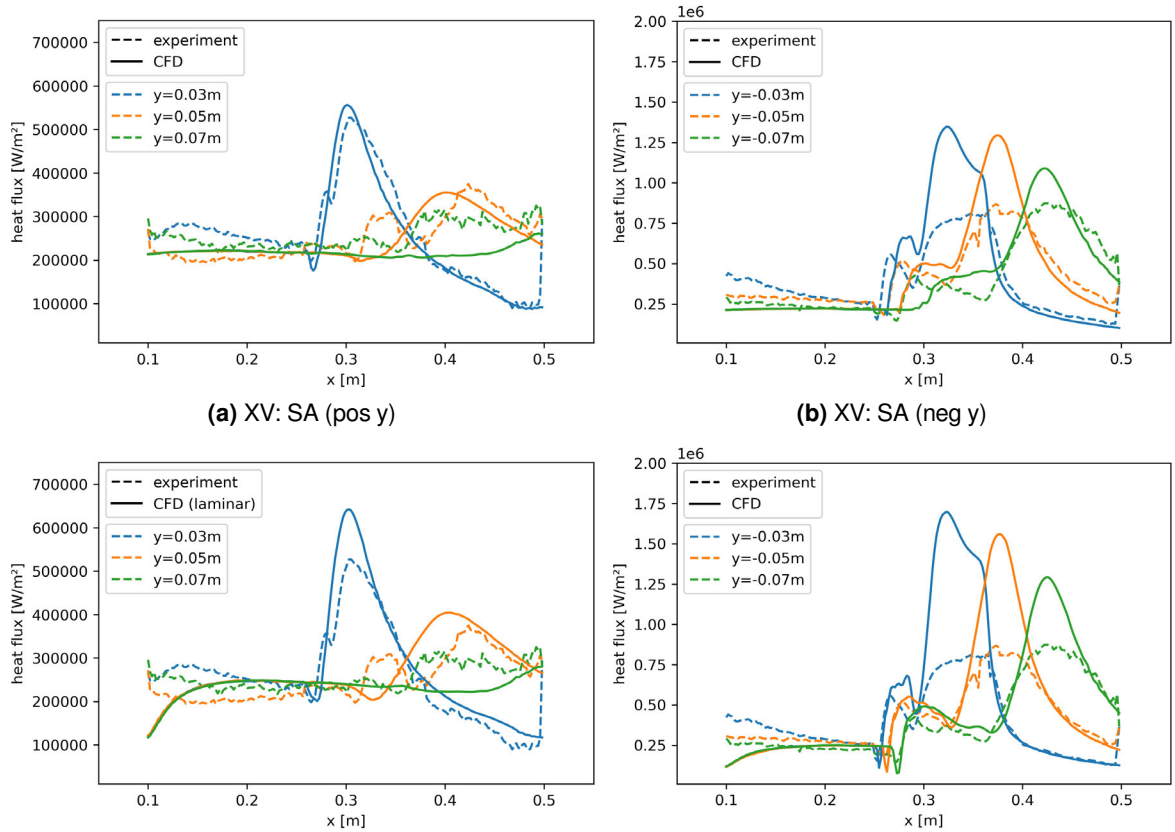

(a) XV: SA (pos y)

(b) XV: SA (neg y)

(c) XV: k-ω SST (pos y)

(d) XV: k-ω SST (neg y)

Figure 15. Heat flux from experimental data and numerical data on constant y coordinate (y = $\mp$ 0.03, 0.05, 0.07) on both sides of the fin. The left column shows the data for positive y coordinates and the right for negative y coordinates. Laminar, SA and k-ω SST turbulence model.

performed and compared for flow topology and turbulence model influence. For 2 configurations (XIII: 0 deg AoF and XV: 15 deg AoF) first preliminary comparisons between experimental and CFD data were conducted. While the XIII condition compares well between experiment and CFD, the XV condition which shows clear signs of transitional flow exhibits rather complex physical phenomena which require further investigation, both experimentally and numerically.

Acknowledgements

We would like to acknowledge Prof. Klaus Hannemann, born on January 31, 1959, in Karlsruhe, Germany, who passed away on September 21, 2021, at the age of 62. His death shocked all his friends, colleagues, and everybody who knew him as a healthy, strong, and active person, and this will be the way we will remember him [17]. The intersection between experiment and numerical work was always a very important topic to him and we would like to remember this work as one of the last internal collaborations he initiated before his passing.

References

1. Watts, J. D. Flight experience with shock impingement and interference heating on the X-15-2 research airplane. *NASA TM X-1669* (1968).
2. Schmisseur, J. D. Hypersonics into the 21st century: A perspective on AFOSR-sponsored research in aerothermodynamics. *Progress in Aerospace Sciences* **72.** Celebrating 60 Years of the Air Force Office of Scientific Research (AFOSR): A Review of Hypersonic Aerothermodynamics, 3–16 (2015).

3. Gülhan, A., Willems, S. & Klingenberg, F. *STORT flight experiment for high speed technology demonstration* in *72nd International Astronatical Congress* (international astronautical federation, Oct. 2021).
4. Kirchhartz, R. & Jung, W. *MORABA Activities in Retrospect: New Flight Test Capabilities & Competences* in *24th ESA Symposium on European Rocket & Balloon programmes and related research* (2019).
5. Ozawa, H., Laurence, S. J., Schramm, J. M., Wagner, A. & Hannemann, K. Fast response temperature sensitive paint measurements on a hypersonic transition cone. *Experiments in Fluids* **56,** 1853 (2014).
6. Schramm, J. M., Hannemann, K., Ozawa, H., Beck, W. & Klein, C. *Development of Temperature Sensitive Paints in the High Enthalpy Shock Tunnel Göttingen, HEG* in *8th European Symposium on Aerothermodynamics for Space Vehicles* (2015).
7. Ozawa, H., Laurence, S. J., Schramm, J. M., Wagner, A. & Hannemann, K. Fast-response temperature-sensitive-paint measurements on a hypersonic transition cone. *Experiments in Fluids* **56.** Published online: 07. Dec. 2014, Article: 1853, 1–13 (2015).
8. Adler, M. C. & Gaitonde, D. V. Influence of separation structure on the dynamics of shock/turbulent-boundary-layer interactions. *Theoretical and Computational Fluid Dynamics* **36,** 303–326 (Apr. 2022).
9. Pickles, J. D., Mettu, B. R., Subbareddy, P. K. & Narayanaswamy, V. On the mean structure of sharp-fin-induced shock wave/turbulent boundary layer interactions over a cylindrical surface. *Journal of Fluid Mechanics* **865,** 212–246 (2019).
10. Smith, N., Levis, M., Norris, J. & Hamner, M. P. in *12th AIAA International Space Planes and Hypersonic Systems and Technologies* ().
11. Hannemann, K., Schramm, J. M., Wagner, A., Friedl, D. & Camillo, G. P. The High Enthalpy Shock Tunnel Göttingen of the German Aerospace Center (DLR). *Journal of large-scale research facilities JLSRF* **4,** 133 (2018).
12. Cook J. C., W. J. & Felderman, E. J. Reduction of data from thin-film heat-transfer gages - A concise numerical technique. *AIAA Journal* **4,** 561–562 (1966).
13. Langer, S., Schwöppe, A. & Kroll, N. The DLR Flow Solver TAU – Status and Recent Algorithmic Developments. *AIAA Paper AIAA-2014-0080. 52nd Aerospace Sciences Meeting* (2014).
14. Spalart, P.R. & Allmaras, S.R. A One-Equation Turbulence Model for Aerodynamic Flows. *AIAA Paper AIAA-92-0439* (1992).
15. Menter, F. R. Two-equation eddy-viscosity turbulence models for engineering applications. *AIAA Journal* **32,** 1598–1605 (1994).
16. Knight, D. D., Horstman, C. C., Shapey, B. & Bogdonoff, S. Structure of supersonic turbulent flow past a sharp fin. *AIAA Journal* **25,** 1331–1337 (1987).
17. Schramm, J. M., Dillmann, A., Hornung, H. G., Ito, K., Grabe, M., Karl, S., Klar, P. J., Morgan, R., Paull, A. & Steelant, J. In memoriam Prof. Klaus Hannemann (1959–2021). *Shock Waves. Springer Nature* (ed SPRINGER) 1–3 (Apr. 2022).